DIELECTRONIC RECOMBINATION OF Mg II IN STELLAR ENVELOPES

Alicia Cruzado[1]

Observatorio Astronómico de La Plata, Paseo del Bosque S/N, 1900-La Plata, Argentina

Héctor O. Di Rocco[2]

Instituto de Física de Arroyo Seco (IFAS), Pinto 399, 7000-Tandil, Argentina

AND

Adela E. Ringuelet

Observatorio Astronómico de La Plata, Paseo del Bosque S/N, 1900-La Plata, Argentina

ABSTRACT

The aim of the present paper is to discuss the significance, in the infrared continuum of Be stars, of the dielectronic recombination (DR) of Mg II atoms. To accomplish this, we have calculated the emissivity in the lines of Mg I atoms after the process of electron capture has taken place. In order to estimate its influence in the photospheric flux, we have considered the total energy emitted in all lines with $\lambda_1 \leq \lambda \leq \lambda_2$, where λ_1 and λ_2 define the wavelength ranges of the Johnson system filters. We conclude that the DR of Mg II atoms does actually contribute significantly to the infrared excess observed in Be stars.

Subject headings: atomic processes — infrared: stars — stars: emission-line, Be

1. INTRODUCTION

The spectrum of Be stars deviates from that of normal B stars throughout all spectral regions. Here we will be concerned with the infrared wavelengths for which the continuum shows, in almost all cases, an excess of radiation relative to theoretical atmospheric models describing early-type spectra.

Two main hypotheses, which are reviewed here, have been advanced to account for this difference. They are as follows:

1. *Thermal reemission of radiation by circumstellar dust particles.*—Pecker (1962, 1963) was the astronomer who hinted that dust particles present in the stellar envelope could give rise to the IR excess observed in young stars. Several large IR excesses of peculiar objects could be fitted to one or more blackbody curves as was done by Swings (1973), Allen (1973), Savage et al. (1978), Sitko & Savage (1980), and Catalá (1983). However, no quantitative models have been worked out to permit a comparison with the observations.

2. *Free-bound and free-free emission produced in a circumstellar envelope of ionized gas.*—In the early contributions by Woolf, Stein, & Strittmatter (1970) and Gehrz et al. (1974), the free-free radiation emitted by a hydrogen plasma at a temperature of 1.5×10^4 K was calculated and the excesses they could explain in that way were very small. Dyck & Milkey (1972) added to this model a cooler envelope and considered ionized metals outside the H II regions as a source of free electrons. Milkey & Dyck (1973) also considered free-bound transitions, accounting for some larger IR excesses with this more detailed atmospheric structure.

The significance of a coronal region for increasing the infrared flux was put forth by Cassinelli & Hartmann (1977). Different structures of the extended atmosphere were analyzed by Waters (1986), Waters, Coté, & Lamers (1987), and Waters et al. (1991) on the basis of free-free and free-bound emission processes. They interpreted the infrared excess in terms of an equatorial disk with opening angle θ and density distribution $\rho(R) = \rho_0(r/R_*)^{-n}$. For the Be stars studied they obtained $2 \leq n \leq 3.5$ and $R_{\mathrm{disk}} > 4.5 \, R_*$. Their results accounted for general trends of IR excesses and described some particular cases.

By means of a rigorous solution of the transfer problem in an extended atmosphere with chromospheric structure, Vázquez, Cidale, & Ringuelet (1993) were able to reproduce infrared excesses of a group of Be stars designated as F in Allen's (1973) classification of IR continua.

All these hypotheses, which considered free-free emission, account for some cases of IR excess observed in Be stars. However, they cannot account for large excesses, such as the ones observed in B[e] stars. Figure 1 shows the photometric observations of two Be stars with large excesses.

The aim of this paper is to suggest a mechanism that may be an important contributor to the IR emission in Be stars, namely, *dielectronic recombination that originated in a cool circumstellar envelope.* Here we investigated the significance of the process of dielectronic recombination of Mg II. The physical conditions in the cool envelope that surrounds Be stars allow dielectronic recombination of Mg II. Since Mg II is mainly in the ground state (as observed in UV spectra), electronic capture produces Mg I atoms in autoionizing levels above the first ionization level, the lifetime of some of these levels being large enough to allow bound-bound transitions to lower levels. In order to evaluate the contribution of this atomic process to the stellar infrared flux, we calculated the emissivity in the lines. To do this, we solved the statistical equilibrium equations for the physical conditions in the envelope and computed transition probabilities of free-bound and bound-bound transitions applying the Hartree-Fock methodology. To check our results with observations, we took into account the response functions of the filters used. The calculations were carried out for different stellar parameters, T_{eff} and R_*, and for different conditions in the envelope, T_e, N_e, and distance to the central star of the region where recombination takes place.

[1] Fellow of the University of La Plata.

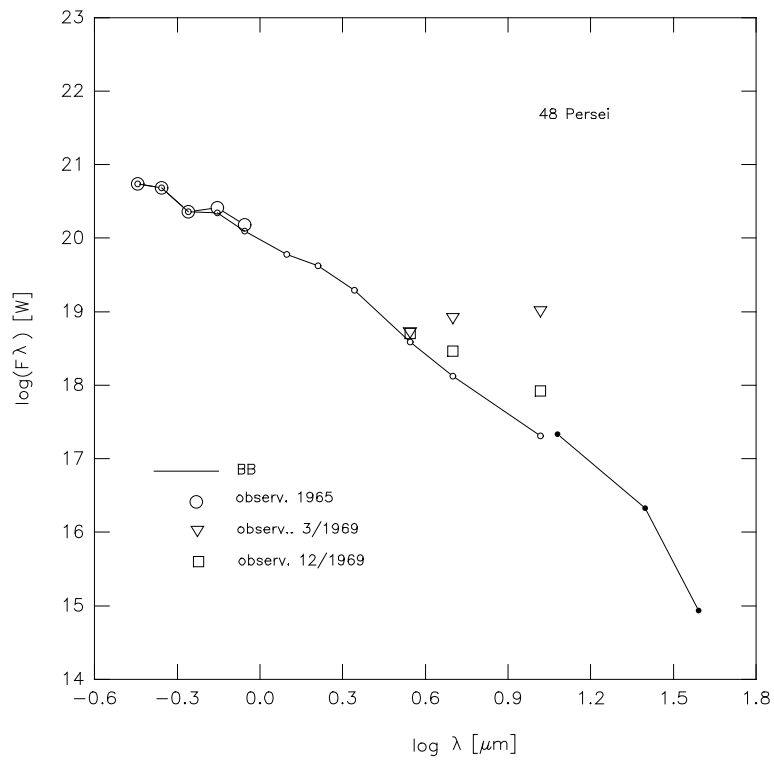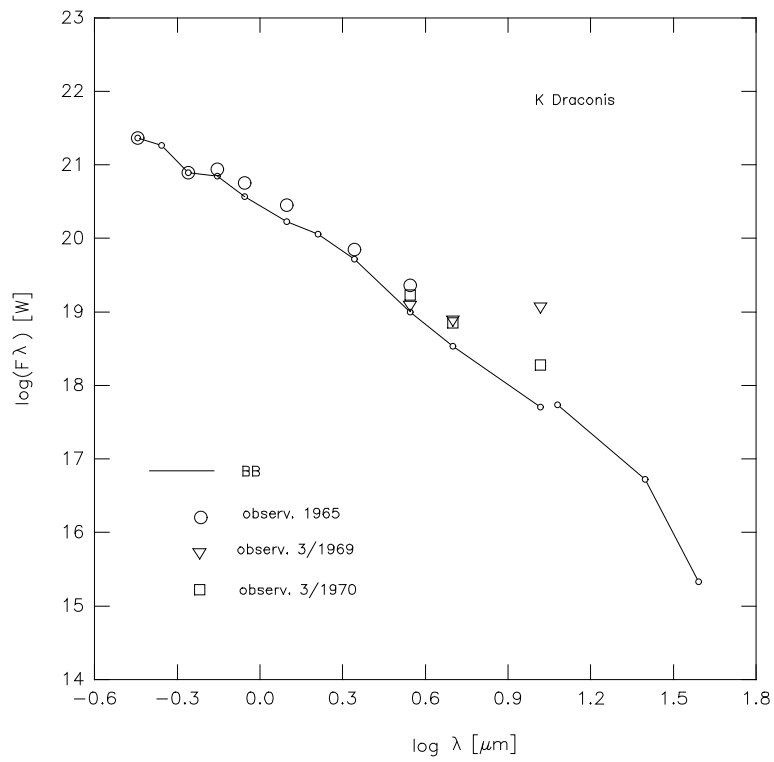[2] Member of the Carrera del Investigador Científico, CONICET, Argentina.

Fɪɢ. 1.—Photometric observations of two Be stars. The BB curve represents blackbody emission.
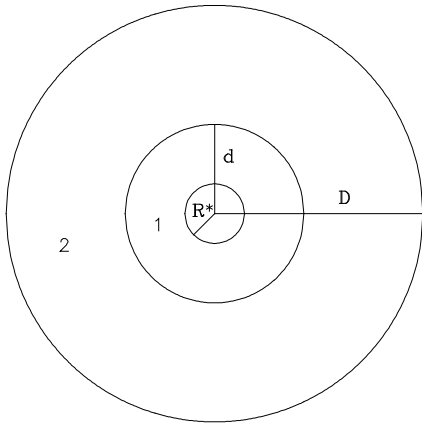
FIG. 2.—Scheme of a Be star and its envelope: hot region (1) and cool envelope where DR occurs (2).

FIG. 3.—Scheme showing the autoionizing and bound states belonging to the two configuration groups.

2. ATMOSPHERIC MODEL ADOPTED

We adopted the stellar atmospheric model proposed by Ringuelet, Fontenla, & Rovira (1981) and developed by Thomas (1983). This model assumes three regions in the Be stars' atmospheres:

1. A photosphere in radiative equilibrium and hydrostatic equilibrium, where temperature and density distribution are given by Kurucz (1979) models.

2. A geometrically thin expanding chromosphere where the temperature reaches a maximum.

3. A cool envelope; in this region the temperature has a constant low value and the electron density drops down smoothly.
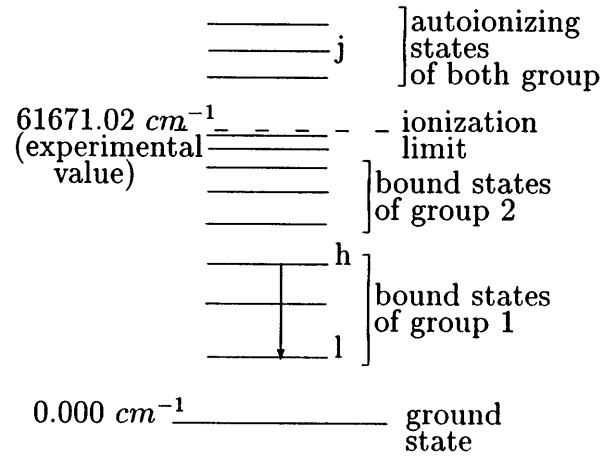
This model has proved to produce consistent results in the calculations of Hα profiles (Cidale & Ringuelet 1993), infrared excesses (Vázquez et al. 1993), and line profiles of resonant transitions of Mg II (Cidale & Ringuelet 1997) and Fe II (Paoli 1996).

3. DIELECTRONIC RECOMBINATION OF Mg II IN THE STELLAR ENVELOPE

Burgess & Seaton (1964) have emphasized the importance of this atomic process in low-density media, and Nussbaumer & Storey (1983, 1984, 1986) have disclosed its effectivity at high and low temperatures. From all the metals, we have chosen the Mg II ion because its abundance
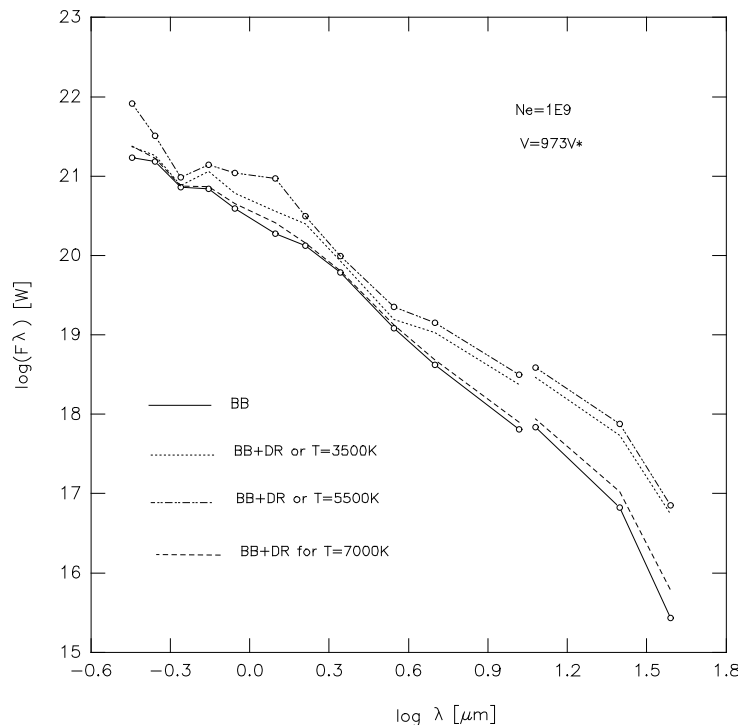

FIG. 4.—Flux distribution vs. wavelength for three different values of the electron temperature: 3500, 5500, and 7000 K. For all curves the electron density has the same value, 10^9 particles cm^{-3}. The value adopted for the emitting volume was $973V*$ ($V*$ = stellar volume). BB represents the photospheric flux calculated with eq. (5). DR represents the flux due to the DR of Mg II calculated with eq. (6).
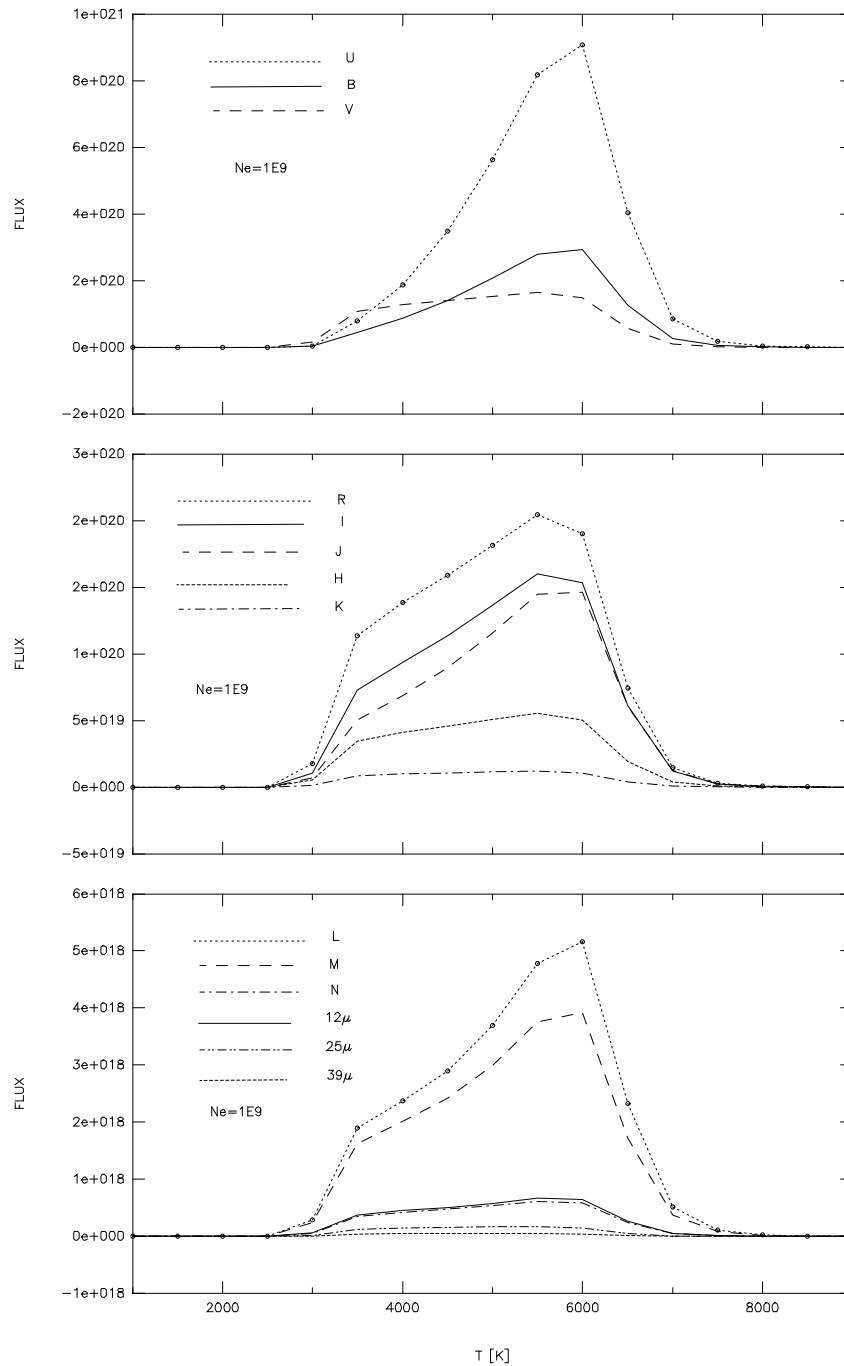
FIG. 5.—Flux distribution with electron temperature for the filter-effective wavelengths of the Johnson system. All the curves were obtained for the same value of the electron density, 10^9 particles cm^{-3}. In this figure we represent, in arbitrary units, only the flux due to the DR of Mg II.

in the fundamental level is very high in the extended atmospheres of Be and B[e] stars, as is suggested by the strength of the UV resonance lines.

In this first analysis, where we have only considered Mg II, we define the envelope as a region with constant density, constant temperature, and a diluted radiation field.

Calculations are performed for values of the parameter N_e(e^- number cm^{-3}) between 10^7 and 10^{11}; the parameter T (temperature) has been given values between 3×10^4 and 10×10^4 K.

According to our atmospheric model, normal Be stars reach such conditions at 3 or 4 stellar radii, where the particle density drops to 10^{-2} the photospheric value, the temperature has values between 3×10^4 and 10×10^4 K, and the radiation field is 1/10 the value at the base of the wind.

Under these conditions, we can neglect all radiatively and collisionally induced processes; consequently, autoionizing levels of the Mg I atom will be populated by dielectronic capture only and depopulated by autoionization or downward radiative transitions.
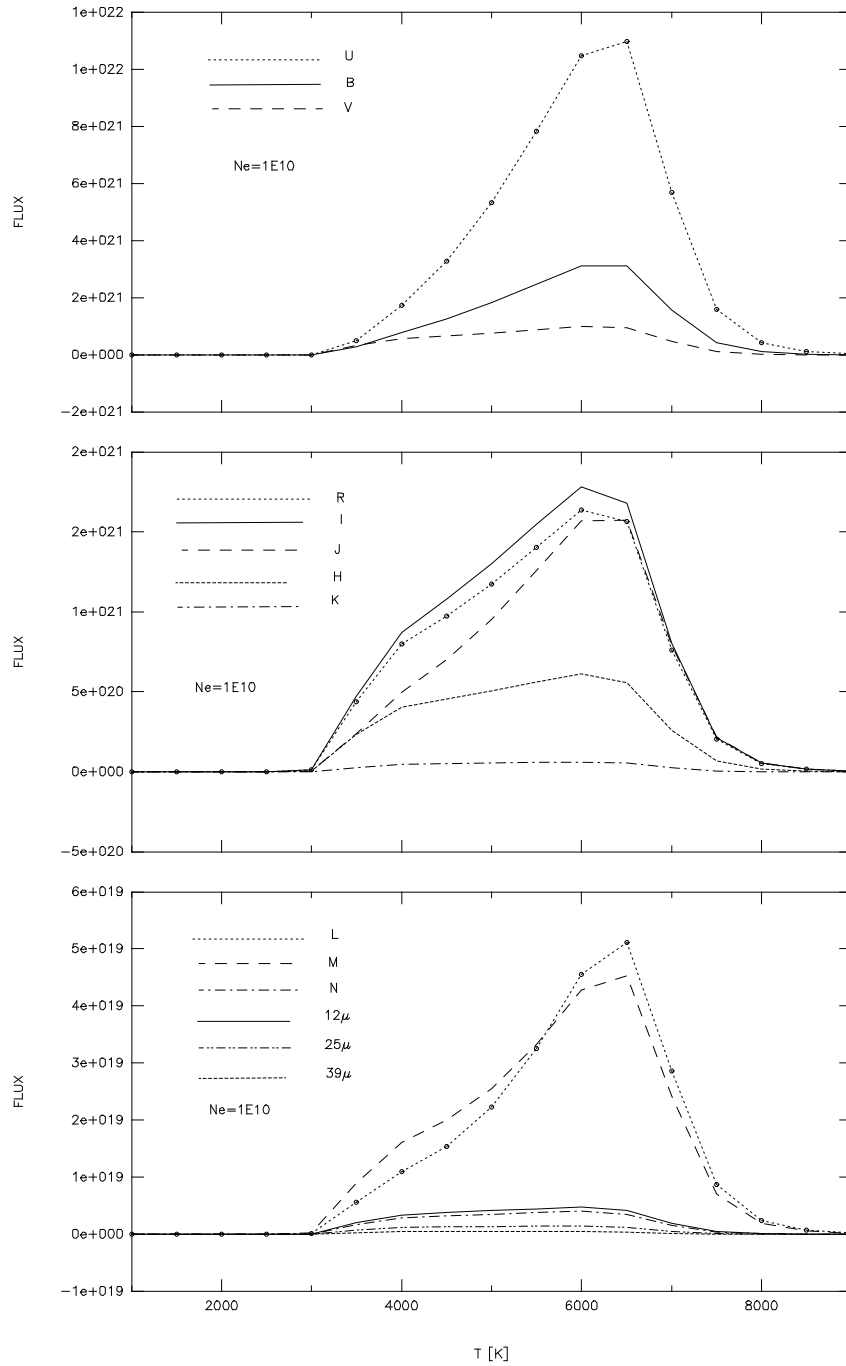
FIG. 6.—Same as Fig. 4, but for $N_e = 10^{10}$ particles cm^{-3}

Next, we solve the statistical equilibrium equations taking into account that Mg II will be mainly in the ground state; thus, we get for the recombination coefficient

$$\alpha_{jh}^D = \frac{N_j^s(\text{Mg I})P_{jh}^R}{N_e\, N^s(\text{Mg II})} \sum_i \frac{P_{ji}^A}{(\sum_i P_{ji}^A + \sum_k P_{jk}^R)}, \qquad (1)$$

where i is the continuum state of the Mg II atom, j is the autoionizing state of the Mg I atom, k and h are the bound states of the Mg I atom, α_{jh}^D is the dielectronic recombination

coefficient for the $j \to h$ transition (cm^3 s^{-1}), N_e is the e^- number per unit volume, $N_j^s(\text{Mg I})$ is the number of Mg I atoms in the j autoionizing state given by the Saha equation, $N^s(\text{Mg II})$ is the number of Mg II atoms given by the Saha equation, P_{ji}^A is the autoionization probability for the $j \to i$ transition (s^{-1}), P_{jk}^R is the radiative probability for the $j \to k$ transition (s^{-1}), and P_{jh}^R is the radiative probability for the $j \to h$ transition (s^{-1}). Furthermore, the quantity $\alpha_{jh}^D N_e N^s(\text{Mg II})$ defines the recombination rate for the j and h states in units of cm^{-3} s^{-1}.

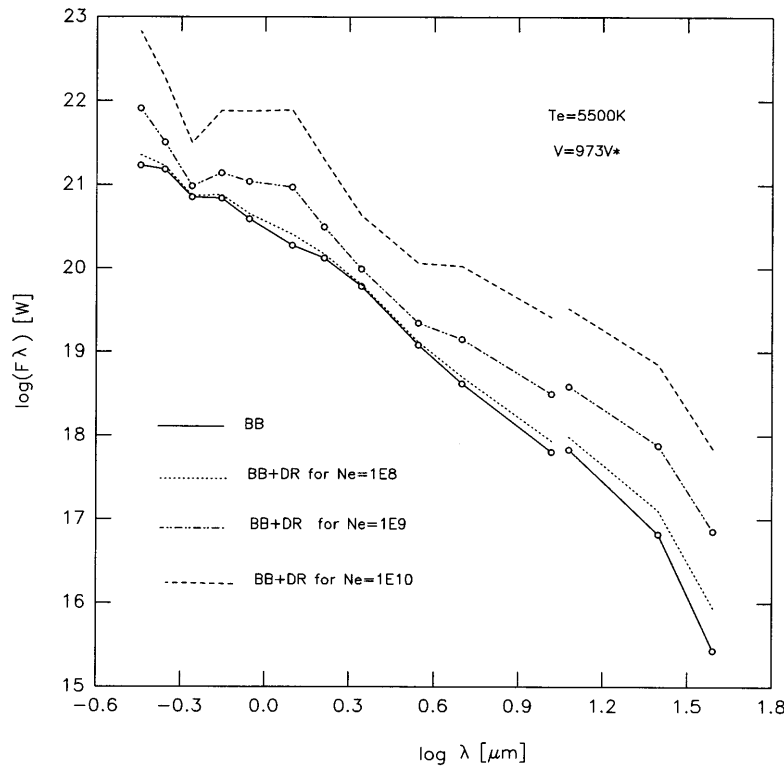Therefore, the effective recombination coefficient of the

FIG. 7.—Flux distribution with wavelength for three different values of the electron density: 10^8, 10^9, and 10^{10} particles cm^{-3}. The same value of the electron temperature, 5500 K, has been adopted for all three curves. For the emitting volume, the adopted value is $973V*$.

line with wavelength λ_{lh} can be written

$$\alpha_{\text{eff}}^D(\lambda_{lh}) = \frac{P_{lh}^R}{\sum_{k<l} P_{lk}^R} \sum_j \alpha_{jh}^D \ . \tag{2}$$

Thus, the emissivity in the line due to recombination is

$$\epsilon(\lambda_{lh}) = N_e N(\text{Mg II})\alpha_{\text{eff}}^D(\lambda_{lh})h\nu_{lh} \ . \tag{3}$$

The calculation of the transition probabilities of Mg I (Burke & Moores 1968; Nussbaumer & Storey 1986) shows that $P^A \gg P^R$ for states permitted to autoionize in LS coupling and that $P^A > P^R$ for states not permitted to autoionize in LS coupling; thus, as a consequence, taking the Saha equation into account, we obtain

$$\epsilon(\lambda_{lh}) = N_e N(\text{Mg II}) \frac{P_{lh}^R}{\sum_{k<l} P_{lk}^R}$$
$$\times \sum_j \left[\frac{g_j}{2g_m} \left(\frac{h^2}{2\pi m KT} \right)^{3/2} e^{-E_j/KT} P_{jh}^R \right] h\nu_{lh} \ ; \tag{4}$$

at low temperatures, it is sufficient that $\sum_j$ would be carried over a few autoionizing levels lying above the first ionization level.

In order to evaluate the contribution to the stellar infrared flux of the energy emitted in the lines, let us look at Figure 2, where we schematize a Be star and its envelope; in zone 2, dielectronic recombination (DR) does occur.

We can calculate the energy emitted by the central star in the $\Delta\lambda = \lambda_2 - \lambda_1$ wavelength interval by means of the following expression:

$$E_* = 4\pi R_*^2 \pi \int_{\lambda_1}^{\lambda_2} B_\lambda d\lambda \ , \tag{5}$$

where B_λ is Planck's function. This expression is in good agreement with the Kurucz models for large wavelengths.

The energy emitted by zone 2 owing to DR of Mg II in the same wavelength interval can be calculated by means of

$$E_{\text{DR}} = \frac{4}{3}\pi(D^3 - d^3) \sum_{\lambda_1}^{\lambda_2} \epsilon(\lambda_{lh}) \ . \tag{6}$$

Here, $\sum_{\lambda_1}^{\lambda_2} \epsilon(\lambda_{lh})$ is run over all the lines with $\lambda_1 \le \lambda \le \lambda_2$.

Then the observed flux, can be written

$$F_0 = \frac{4\pi^2 R_*^2 \int_{\lambda_1}^{\lambda_2} B_\lambda d\lambda + (4/3)\pi(D^3 - d^3) \sum_{\lambda_1}^{\lambda_2} \epsilon(\lambda_{lh})}{4\pi D_{\text{ob}}^2} \ , \tag{7}$$

where D_{ob} is the distance to the observer.

4. METHODOLOGY

We calculated equation (7) for the color filters wavelength intervals of the Johnson system without considering the distance to the observer. To do this, we need to compute the term energies of the bound and autoionizing states of the Mg I atom (E), the wavelength of the possible transitions (λ_{lh}), and its radiative transition probabilities (P^R). The required one-electron radial functions were calculated with the Hartree-Fock method. The calculations were carried out in intermediate coupling with the Cowan (1993) code.

Because of computer limitations, the calculations were performed with a limited number of electronic configurations and a limited number of electronic subshells. Therefore, we have proceeded in two stages, with two different groups of atomic configurations:

1. In the first group are atomic configurations giving origin to bound states with $1 \le n \le 12$ and $0 \le l \le 3$ (hereafter group 1).
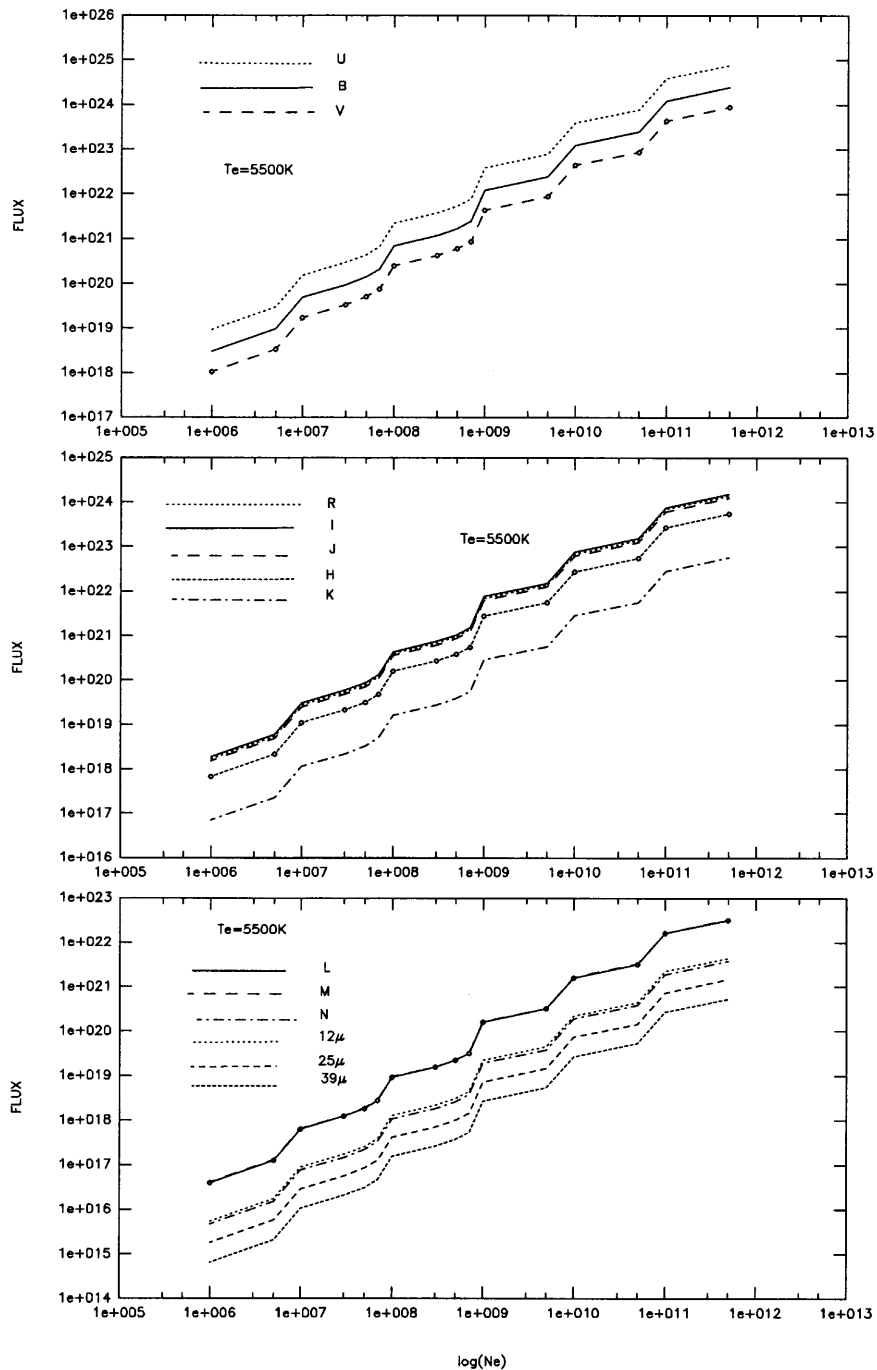
FIG. 8.—Flux distribution with electron density for the filter-effective wavelengths of the Johnson system. All the curves were obtained for the same value of the electron temperature, 5500 K. In this figure we represent, in arbitrary units, only the flux due to the DR of Mg II.

2. In the second group are atomic configurations giving origin to bound states with $13 \leq n \leq 22$ and $0 \leq l \leq 3$ (hereafter group 2).

In both groups the atomic configurations giving rise to autoionizing states have $3 \leq n \leq 6$ and $0 \leq l \leq 2$.

The energy levels originated in the atomic configurations[3] of both groups are depicted in Figure 3.

[3] The theoretical values of the energy levels differ from the experimental values; they are all shifted by a similar amount, and since our calculations involve only differences between energy levels, no important errors are introduced.

Our calculation gave, for the first configuration group, 7726 lines with 0.1 μm $\leq \lambda \leq 50$ μm and 6638 lines for the second group in the same wavelength range. We have calculated the emissivity in the lines resulting from transitions between bound states; there are 2137 lines resulting from these transitions with wavelengths in the interval 0.16 μm $\leq \lambda \leq 50$ μm for group 1 and 476 lines with wavelengths in the interval 6.5 μm $\leq \lambda \leq 50$ μm for group 2 (there are no lines that originated in transitions between the bound states of group 2 whose wavelengths were shorter than 6.5 μm).

We have investigated the behavior of the emitted IR flux with different parameters of the envelope and for each con-
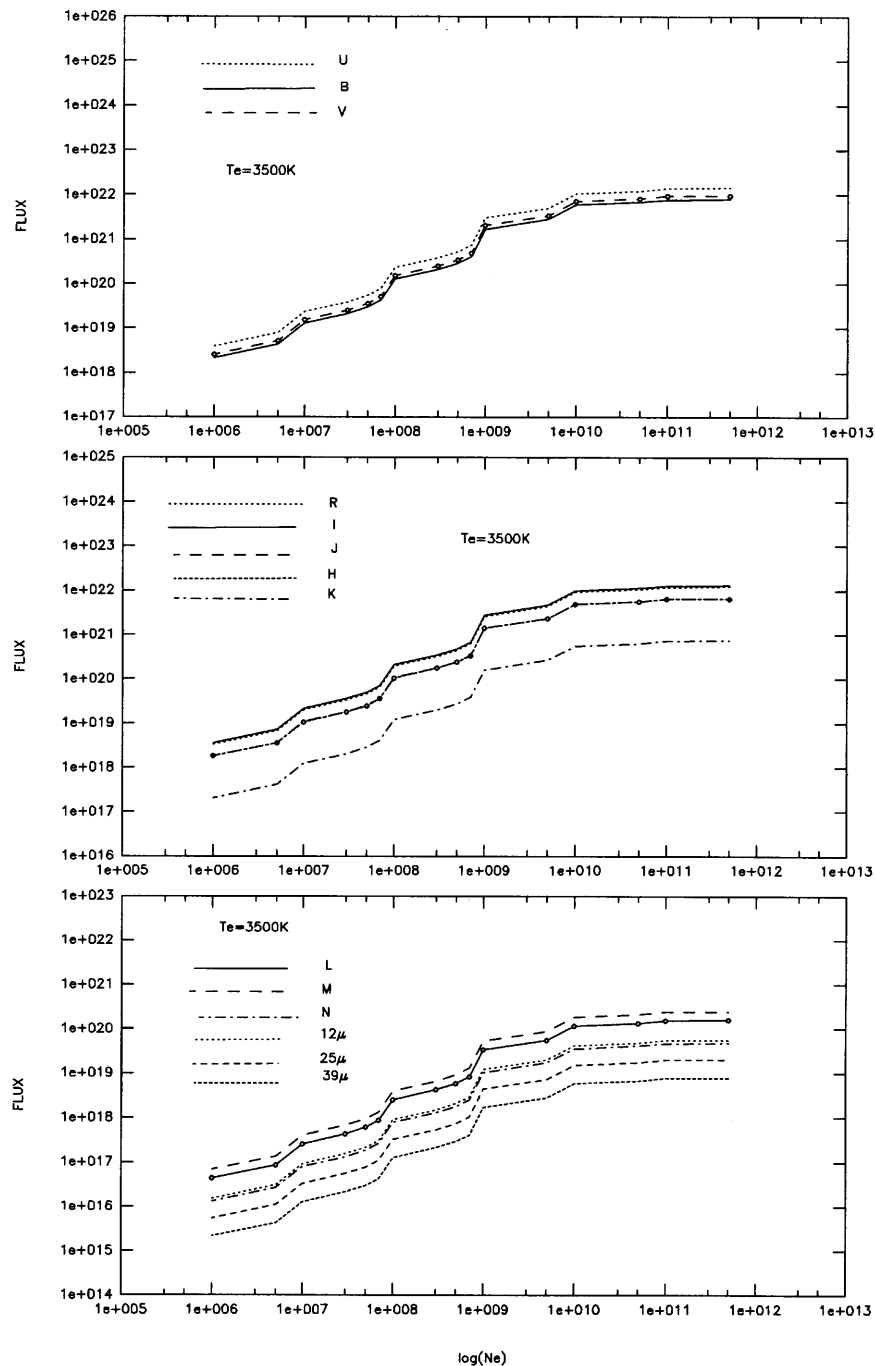
FIG. 9.—The same as Fig. 7, but for $T_e = 3500$ K

figuration group, the stellar parameters remaining fixed ($T_{eff} = 13,500$ K, $R_* = 4\,R_\odot$).

5. RESULTS

5.1. Group 1

5.1.1. Behavior of the Emission When Modifying the Electron Temperature

In Figure 4 we illustrate the emitted flux for three electron temperature values; $\log \lambda$ is the logarithm of the wavelength (in microns) and $\log (F_\lambda \lambda)$ is the logarithm of the total flux multiplied by the wavelength in watts (see Appendix). In Figures 5 and 6 the flux is plotted against electron tem-

perature for the different filter wavelengths; the electronic density being 10^9 in Figure 4 and 10^{10} in Figure 5. In Figures 5 and 6 we observe that the behavior of the flux is similar for all the filters: it increases with temperature until reaching a maximum value and then it decreases; when the electron density changes, the temperature for which the flux has a maximum does shift.

5.1.2. Behavior of the Emission When Modifying the Electron Density

Figure 7 shows the emitted flux for three electron density values. In Figures 8 and 9 we have plotted the flux against electron density for the different filter wavelengths and for
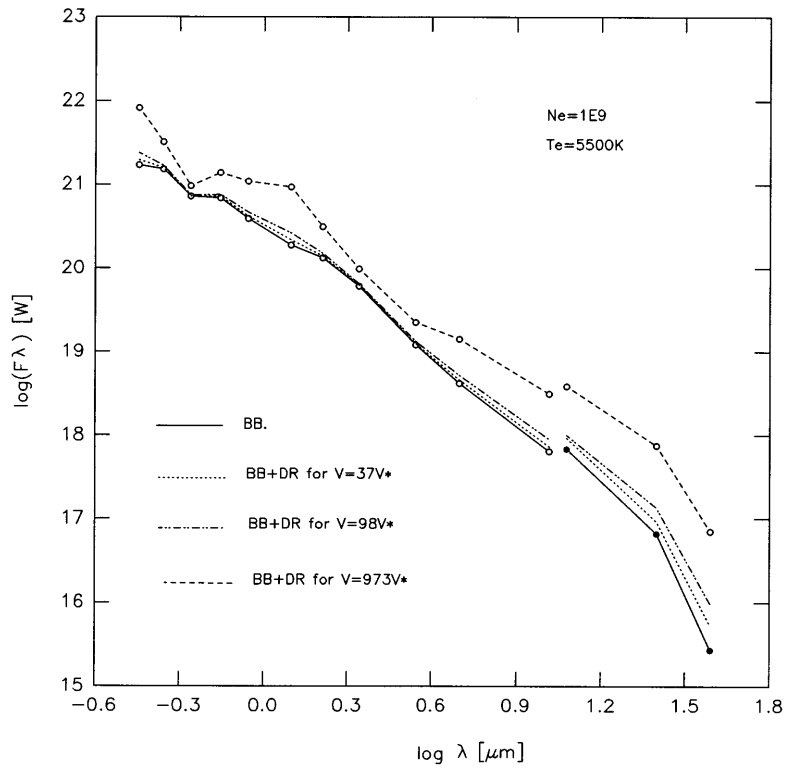
Fig. 10.—Flux distribution with wavelength for three different values of the emitting volume: $37V^*$, $98V^*$, and $973V^*$. The same value for the electron temperature has been adopted for all the curves, 5500 K; the electron density is 10^9 particles cm^{-3}.
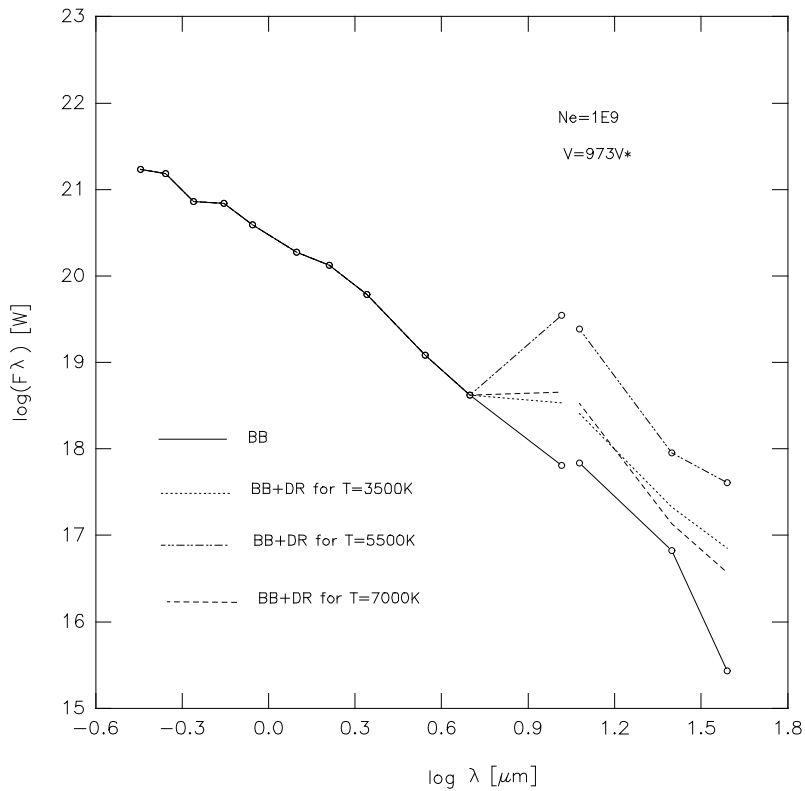

Fig. 11.—Flux distribution with wavelength for three different values of the electron temperature: 3500, 5500, and 7000 K; $N_e = 10^9$ particles cm^{-3} and $V = 973V^*$.
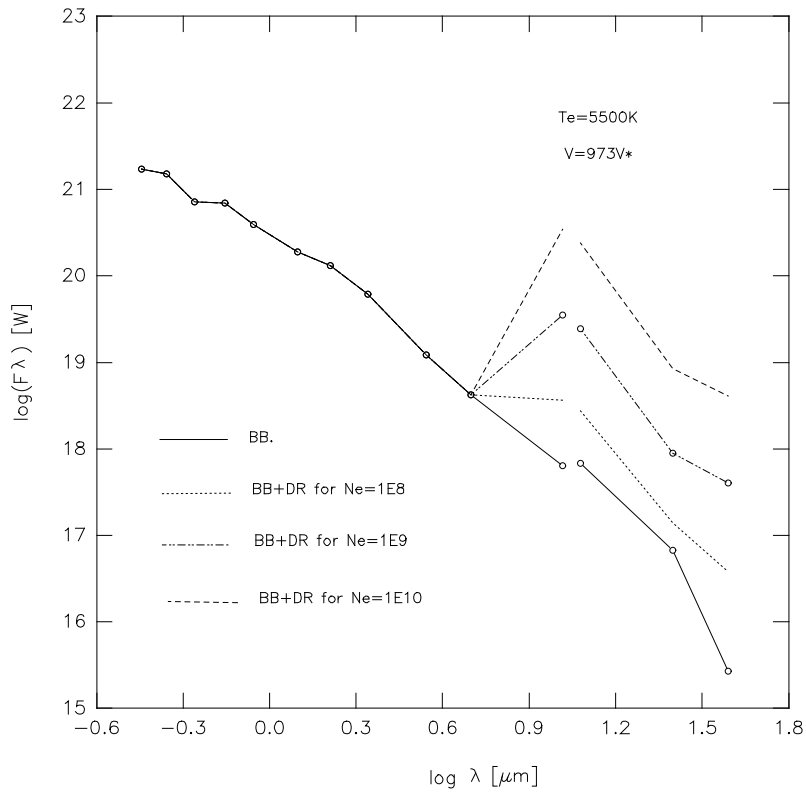
910

FIG. 12.—Flux distribution with wavelength for three different values of the electron density: $N_e = 10^8$, 10^9, and 10^{10} particles cm^{-3}; $T_e = 5500$ K; and $V = 973V^*$.
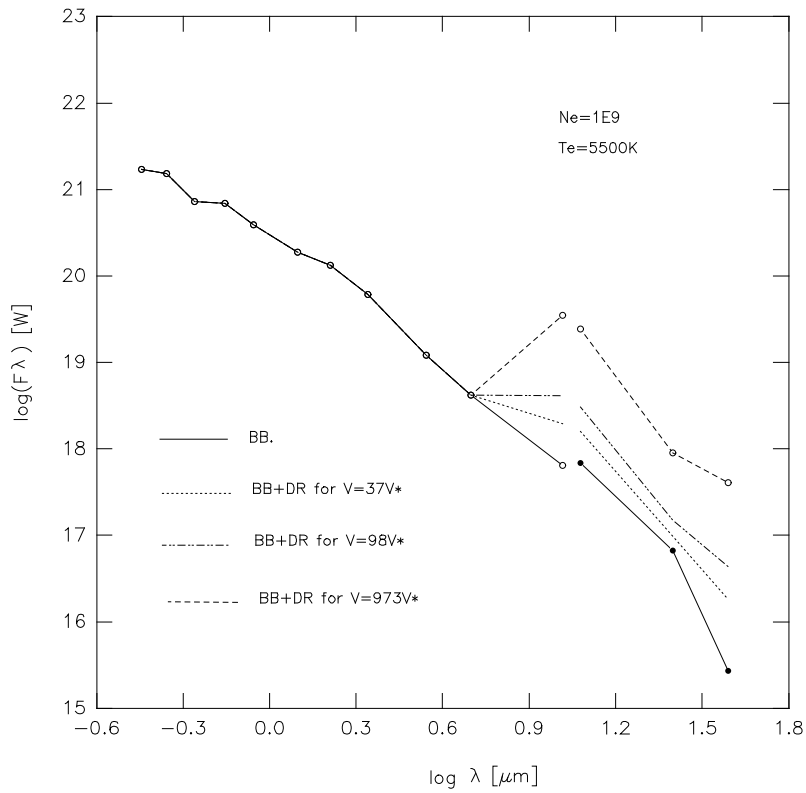

FIG. 13.—Flux distribution with wavelength for three different values of the emitting material volume: $V = 37V^*$, $98V^*$, $973V^*$; $T_e = 5500$ K; and $N_e = 10^9$ particles cm^{-3}.
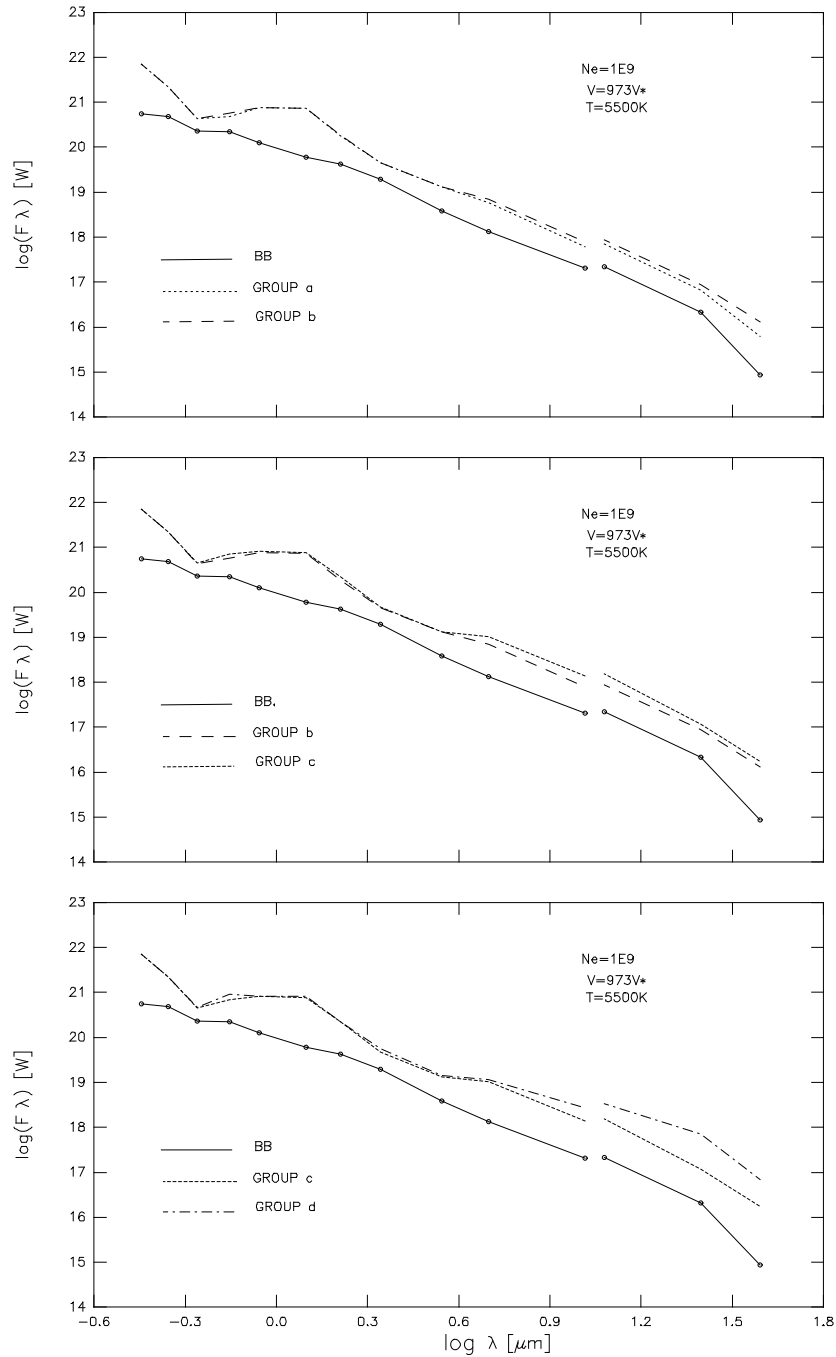
Fig. 14.—Flux distribution with wavelength for four groups of configurations giving origin to bound states. Group *a* is formed with the configurations of group 1 with $n \leq 8$; the same for group *b* with $n \leq 9$, for group *c* with $n \leq 10$, and for group *d* with $n \leq 11$. Groups *a*, *b*, *c*, and *d* include all the configurations giving origin to autoionizing states.

two electron temperature values; the flux is an increasing function of the electron density for the considered values.

5.1.3. *Behavior of the Emission When Modifying the Emitting Volume*

The emitted flux is directly proportional to the volume of the emitting material. The *V*-values in Figure 10 can be obtained from different values of the parameters *d* and *D*, as can be seen in Table 1.

5.2. *Group 2*

To evaluate equation (4) for this second group we have

TABLE 1

POSSIBLE VALUES OF *d* AND *D*[a]
(IN R_*)

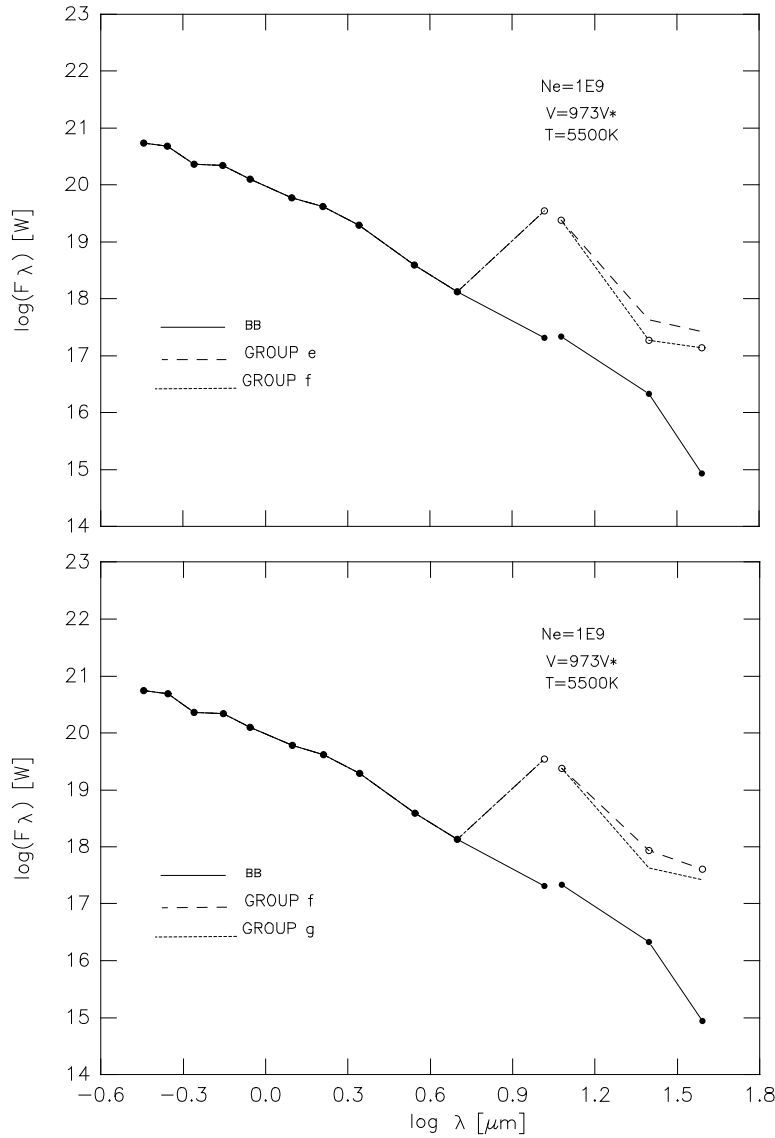| $V = 98V^*$		$V = 973V^*$	
d	*D*	*d*	*D*
3	5	3	10
5	6	5	10.32
10	10.3	10	12.54

[a] With $V^* = $ stellar volume.

FIG. 15.—Flux distribution with wavelength for three groups of configurations giving origin to bound states. Group *e* designates the configurations of group 2 with $n \leq 19$, group *f* includes group 2 with $n \leq 20$, and group *g* includes group 2 with $n \leq 21$. Groups *e*, *f*, and *g* included all the configurations giving origin to autoionizing states.

calculated $\sum_{k<l} P_{lk}^R$ in an approximate form. Since we do not have the values of P_{lk}^R, we have used the hydrogenic approximation

$$A = \frac{1.57E10Z_c^4}{n_i\, n_j^3 (n_j^2 - n_i^2)} \qquad (8)$$

for calculating the preceding sum. In equation (8) we have replaced the total quantum numbers n_i and n_j by the corresponding effective quantum number, in order to adapt it to a nonhydrogenic atom.[4] The behavior of the flux with the different parameters is similar to the behavior of group 1. In Figures 11, 12, and 13, the flux distribution with wavelength is plotted for three values of the electron temperature, three

values of electron density, and three values of the emitting volume, respectively.

5.3. *Contribution of the Individual Configurations*

In order to estimate the flux behavior with the atomic configuration, we have worked them out individually. We can see the results in the following figures that show the influence of some atomic configurations giving origin to bound states, Figures 14 and 15, and to autoionizing states, Figures 16 and 17.

We observe that, within each group, as n increases, the new configurations contribute mainly to longer wavelengths, i.e., as n increases the energy levels get closer and transition probabilities to lower levels decrease with increasing Δn. Among the configurations giving rise to autoionizing states, we verify[5] that $3p^2$, $3p3d$, and $3p4p$ give

---

[4] We have calculated $\sum_{k<l} P_{lk}^R$ for group 1 with eq. (8) and with the values of P_{lk}^R obtained from Cowan's code. Then we compared the calculated emitted flux with both expressions: the maximum difference between both curves is 20% (the mean value of the difference is 8%). We inferred that eq. (8) is a good approximation for our purpose.

[5] The $3p^2$ configuration gives origin to energy levels lying above and below the ionization limit; we have distinguished among them in the calculations.
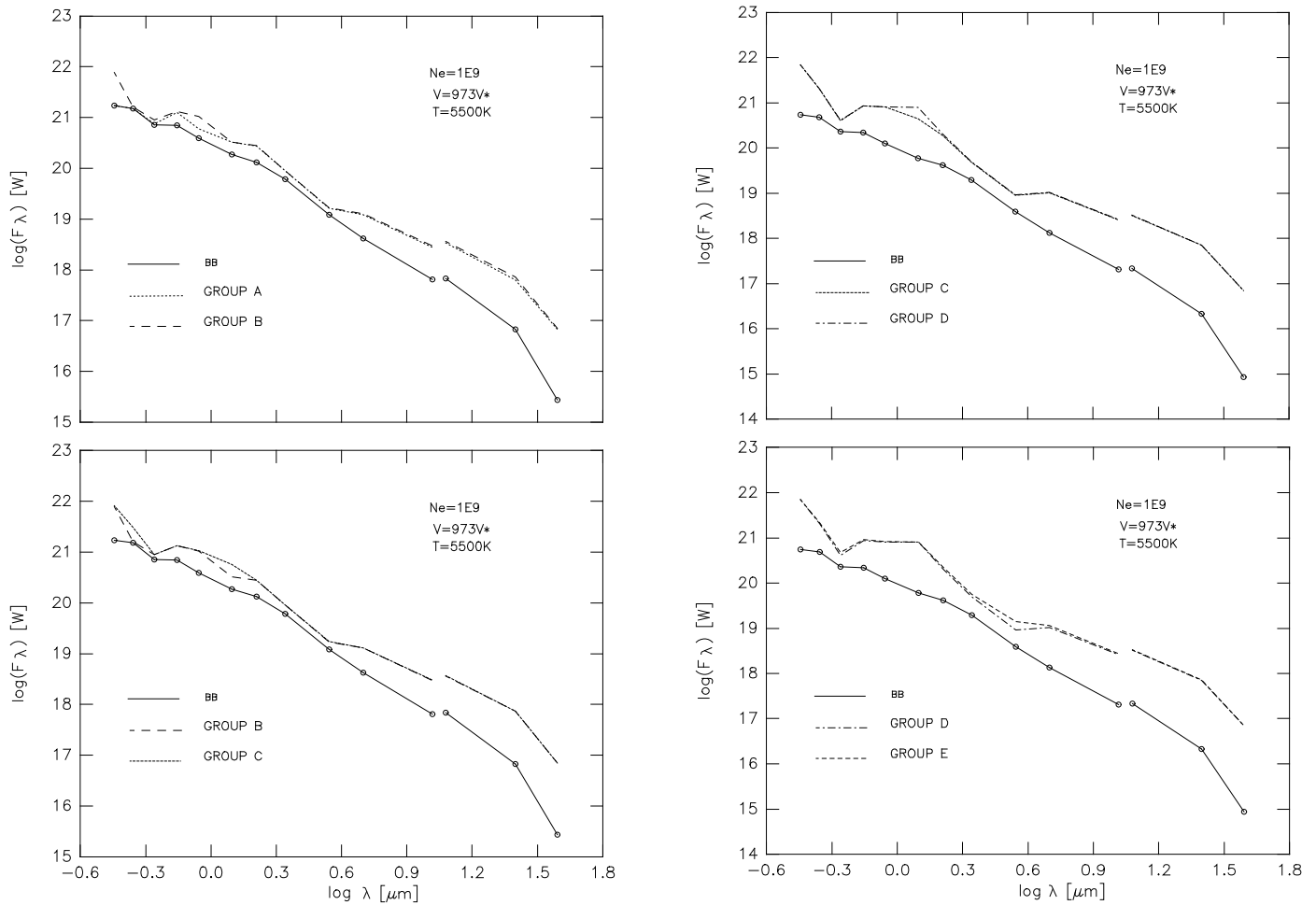
FIG. 16.—Flux distribution with wavelength for five groups of configurations giving origin to autoionizing states. Groups A, B, C, D, and E include all the configurations giving origin to bound states of group 1 and the following configurations giving origin to autoionizing states: group A: $3p^2$; group B: $3p^2$ and $3p3d$; group C: $3p^2$, $3p3d$, and $3p4s$; group D: $3p^2$, $3p3d$, $3p4s$, and $3p4p$; group E: $3p^2$, $3p3d$, $3p4s$, $3p4p$, $3p4d$, $3p5s$, $3p5p$, and $3p5d$.

the greater contribution to the flux. In order to obtain the contribution due to all the configurations of group 1 and group 2, we would have to add the contributions of both groups and, in addition, consider all possible lines between the corresponding states.

6. SUMMARY AND CONCLUSIONS

We have studied the influence of the Mg II dielectronic recombination process in the infrared stellar flux. Ours is a zero-order approximation where we have neither considered the radiative transfer problem nor included the totality of the transitions between intermediate levels; we have adopted a spherical geometry and the Saha population distribution. Nevertheless, we can say that the Mg II dielectronic recombination does really contribute to the infrared stellar flux. The physical conditions in the stellar envelope will determine which atomic configurations contribute to the flux. The electron temperature will determine the amount of autoionizing states reached by the free electrons; the corresponding configurations chosen by us are consistent with the electron temperature interval assumed in this work. The electron density will determine the number of bound states that will suffer a radiative decay before a collisionally induced process. We can estimate the maximum value for the principal quantum number for

which this is true by using the following expression:

$$n_t^7 = \frac{5.6E17(Z-N+1)^6 T^{1/2}}{N_e} .$$

The number of configurations used in our calculation is sufficient if $n_e > 10^{10}$, as is shown by the resulting n_t calculated with equation (8) and taking into account the range in T_e and N_e adopted here.

If $n_e < 10^{10}$ we would have to consider a larger number of levels with high n, which, in turn, would imply additional emission at very large wavelengths.

The adopted values for V are such that they make the DR emission (depending on T_e and N_e) match the photospheric flux at $\lambda \approx 1$ μm.

We are planning to apply our theory to some particular stars. In order to do this, our first step will be to adjust the atomic theoretical parameters so that the computed energy levels could be in good agreement with experimental values (the Cowan code allows us to do this). Moreover, we would like to work with all configurations (first and second groups) at the same time; this will allow us to reduce errors[6]

---

[6] In working with the second group, errors are larger because the unbalance between configurations is more pronounced.
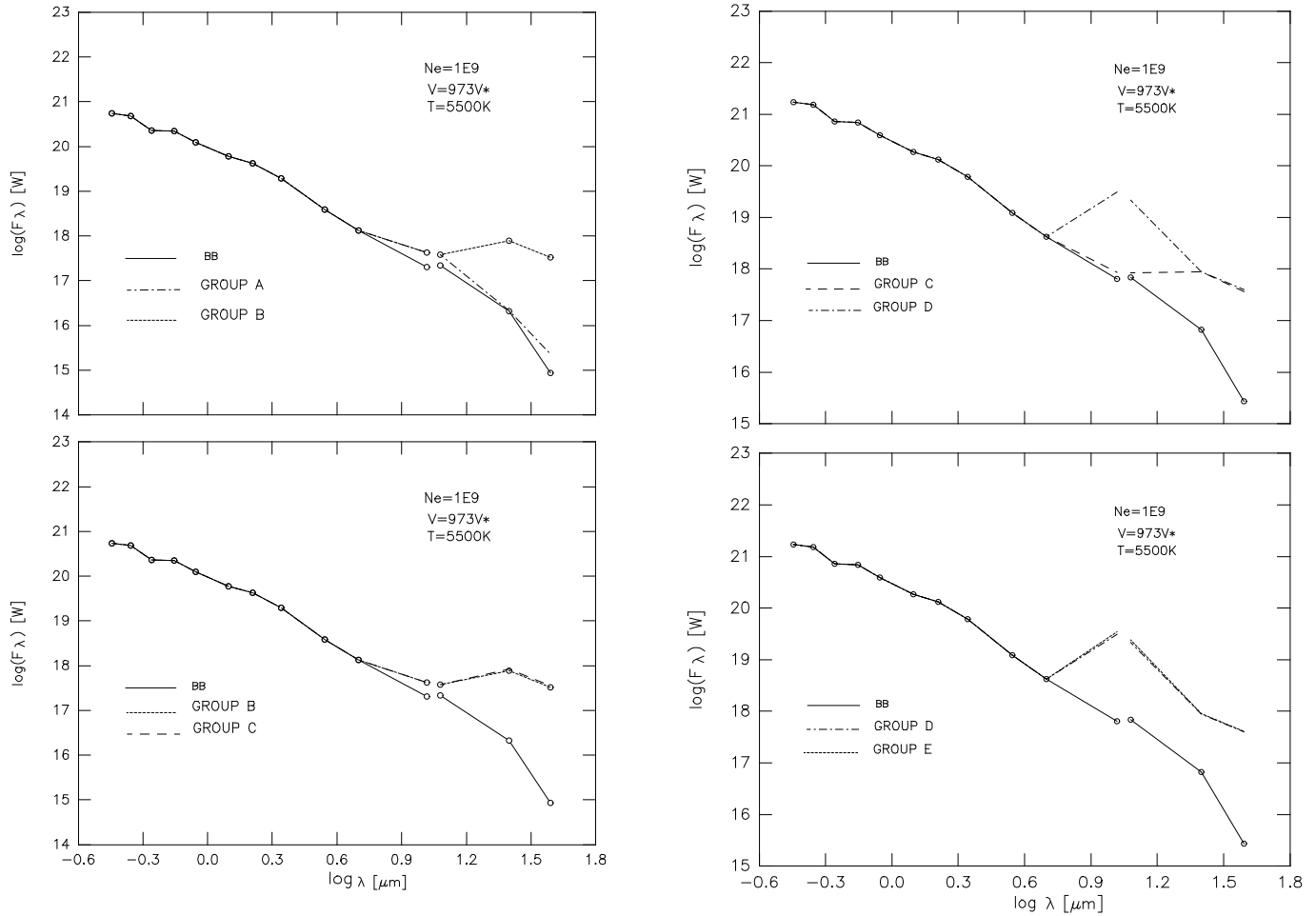
FIG. 17.—Same as Fig. 15, but for group 2

in the calculation of transition probabilities and to take into account all possible transitions between bound levels. We will also consider slab structures that would satisfy, simultaneously, polarimetric results. Furthermore, work is in progress to consider the possible relevance of DR in other atomic species; Fe II and Si II will be our next targets.

APPENDIX

The two terms in the numerator of equation (7) represent an integrated flux between λ_1 and λ_2; therefore we can write

$$4\pi^2 R_*^2 \int_{\lambda_1}^{\lambda_2} B_\lambda \, d\lambda + \tfrac{4}{3}\pi(D^3 - d^3) \sum_{\lambda_1}^{\lambda_2} \epsilon(\lambda_{lh}) \simeq \sum_{\lambda_1}^{\lambda_2} F_\lambda \Delta\lambda_{1,2} \; .$$

Then we can consider

$$F_\lambda \lambda = \frac{\sum_{\lambda_1}^{\lambda_2} F_\lambda \Delta\lambda_{1,2}}{\Delta\lambda_{1,2}} \lambda_{\mathrm{eff}} \; ,$$

where λ_{eff} is the effective wavelength of the corresponding filter.

REFERENCES

Allen, D. A. 1973, MNRAS, 161, 145
Burgess, A., & Seaton, M. J. 1964, MNRAS, 127, 355
Burke, P. G., & Moores, D. L. 1968, J. Phys., 2, 1
Cassinelli, J. P., & Hartmann, L. 1977, ApJ, 212, 488
Catalá, C. 1983, A&A, 125, 313
Cidale, L., & Ringuelet, A. E. 1993, ApJ, 411, 874
———. 1997, preprint
Cowan, R. D. 1981, The Theory of Atomic Structure and Spectra (Berkeley: Univ. California Press)
Dyck, H. M., & Milkey, R. W. 1972, PASP, 84, 501
Gehrz, R. D., Hackwell, J. A., & Jones, T. W. 1974, ApJ, 197, 675
Kurucz, R. L. 1979, ApJS, 40, 1
Milkey, R. W., & Dyck, H. M. 1973, ApJ, 181, 83
Nussbaumer, H., & Storey, P. J. 1983, A&A, 126, 75
———. 1984, A&AS, 56, 293
———. 1986, A&AS, 64, 545

Paoli, S. 1996, preprint
Pecker, J. C. 1962, Space Res., 3, 1076
———. 1963, Space Sci. Rev., 1, 729
Ringuelet, A. E., Fontenla, J. M., & Rovira, M. 1981, A&A, 100, 79
Savage, B. D., Wesselius, P. R., Swings, J. P., & Thé, P. S. 1978, ApJ, 224, 149
Sitko, M. L., & Savage, B. D. 1980, ApJ, 237, 82
Swings, J. P. 1973, A&A, 26, 443
Thomas, R. N. 1983, Stellar Atmospheric Structural Patterns (Greenbelt: NASA SP-47)
Vázquez, A., Cidale, L., & Ringuelet, A. E. 1993, A&A, 419, 286
Waters, L. B. F. M. 1986, A&A, 162, 121
Waters, L. B. F. M., Coté, J., & Lamers, H. J. G. L. M. 1987, A&A, 185, 206
Waters, L. B. F. M., van der Veen, W. E. C. J., Taylor, A. R., Marlborough, J. M., & Dougherty, S. M. 1991, A&A, 244, 120
Woolf, N. J., Stein, W. A., & Strittmatter, P. A. 1970, A&A, 9, 252